Analysis of spatial–temporal converters for all-optical communication links

Dan M. Marom, Pang-Chen Sun, and Yeshaiahu Fainman

We analyze parallel-to-serial transmitters and serial-to-parallel receivers that use ultrashort optical pulses to increase the bandwidth of a fiber-optic communication link. This method relies on real-time holographic material for conversion of information between spatial and temporal frequencies. The analysis reveals that the temporal output of the pulses will consist of chirped pulses, which has been verified experimentally. When the signal pulses are transmitted along with a reference pulse, the distortions of the received signal, caused by dispersion and other factors in the fiber, are canceled because of the phase-conjugation property of the receiver. This self-referencing scheme simplifies the receiver structure and ensures perfect timing for the serial-to-parallel conversion. © 1998 Optical Society of America

OCIS codes: 190.4380, 190.5040, 320.5540, 060.4230, 070.6020.

1. Introduction

Ultrashort pulse shaping by Fourier synthesis in the temporal frequency domain has been extensively investigated in the past decade.[1,2] Spectral holography has expanded the concept of holography to signals in the time domain. The recording of the interference of a signal pulse and a reference pulse permits later readout by an ultrashort pulse and correlation and convolution of ultrafast signals in the optical domain.[3,4] Spectral holography has utilized the duality between the temporal and the spatial frequencies to convert information from pulsed optical signals to cw and vice versa. The interference of spatial frequency information on a hologram can be read out in time by an ultrashort pulse's spectral frequency components for space-to-time conversion.[5] The interference of temporal frequency components of copropagating optical pulses can be recorded as a spectral hologram and read out by diffraction of a cw optical wave for time-to-space conversion.[6] Based on these techniques, transmission of spatial information by means of a temporal channel has been performed[7]: A sequence of cw point sources has been converted to a packet of pulses with a space-to-time setup (parallel-to-serial transmitter) and converted back to the spatial domain with a time-to-space setup (serial-to-parallel receiver). Other methods of performing time-to-space and space-to-time conversions by use of excitonic and second-order nonlinearities have been reported as well.[8–11] The analysis of a spectral decomposition system used in these experiments usually assumes a linear angular dispersion device, the paraxial approximation, and a short optical pulse with a bandwidth that is small compared with the optical carrier frequency.

In this paper a parallel-to-serial transmitter and a serial-to-parallel receiver are analyzed without the limiting assumption that the bandwidth of the pulse is small compared with the optical carrier frequency. The results of this analysis, presented in Section 2, show that the pulses at the output of the transmitter are chirped, with the chirp increasing for shorter pulses or a greater time delay relative to the incident pulse. The performance of the four-wave-mixing (4WM) receiver is shown analytically to be unaffected by the chirped pulses when these pulses are transmitted through an idealized distortionless medium for data recovery in the spatial domain. In practice, these signal pulses will be transmitted through an optical fiber that possesses dispersion and random phase variations due to ambient conditions, thereby affecting the perfect signal recovery in the spatial domain at the receiver. To overcome the fiber dispersion effect, we send the reference pulse along with the data pulses, as described in Section 3. Thus the

The authors are with the Department of Electrical and Computer Engineering, University of California, San Diego, La Jolla, California 92093-0407.

Received 18 August 1997; revised manuscript received 8 January 1998.

0003-6935/98/142858-11$15.00/0

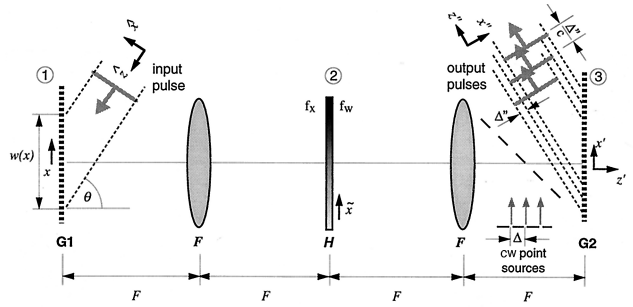

Fig. 1. Structure of the parallel-to-serial transmitter. cw writing beams emanating from point sources separated by Δ propagate from right to left, coupled in by a beam splitter (dashed line). An incident short pulse propagates from left to right, with the spectrum spatially dispersed at plane 2 (by a grating in plane 1), where a real-time 4WM process mixes the cw interference (with reference source not shown) and the pulsed spectrum.

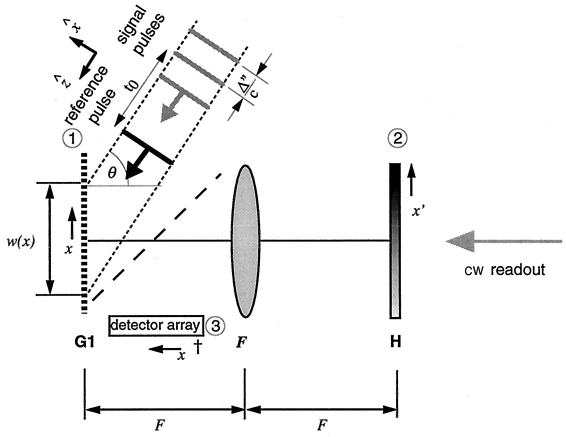

Fig. 2. Structure of the serial-to-parallel receiver. The incoming data pulses are shown in gray, the reference pulse in black. Real-time hologram at plane 2 transfers interference information of the pulses to a readout cw beam. The output cw signal is coupled out by a beam splitter (dashed line) and is focused onto a detector array at output plane 3.

phase distortion of the channel, sampled by the reference pulse, is compensated for at the receiver by means of the phase-conjugation process, when interfered with by the data pulses. An estimate of the aggregate bit-rate capacity of this transmission method is carried out in Section 4 for Gaussian input pulses. In Section 5 we verify experimentally that the output pulses are chirped, as predicted by the analysis, by performing their cross-correlation measurements with a transform-limited pulse. We conclude with a summary in Section 6.

2. Analysis of a Communication Link Based on Ultrashort Pulses

The analysis of the parallel-to-serial transmitter and serial-to-parallel receiver is carried out in the mixed temporal–spatial frequency domain. A real-time hologram by 4WM of cw spatial frequencies and temporal frequencies from ultrashort pulsed waves is used. The transfer of information from the spatial domain to the temporal domain and vice versa is accomplished through the interchangeability of the spatial frequencies' and the temporal frequencies' information for signals in spatial and temporal domains, respectively.

The parallel-to-serial transmitter is based on real-time 4WM in the frequency domain. The temporal frequency spectrum of an incident ultrashort pulse is modulated by a sequence of linear phase functions created by the interference of a signal sequence of cw point sources and a reference point source from the spatial channel (see Fig. 1). The resultant temporal channel output is a sequence of ultrashort pulses shifted in the time domain according to the slope of the corresponding linear phase function from the spatial frequency domain. Further details of the operation are discussed in Subsection 2.A. The information-carrying pulses and the reference ultrashort pulse are transmitted to the receiver for detection.

The serial-to-parallel receiver, shown in Fig. 2, transforms the signal information back to the spatial channel by a second 4WM process. The interference of the information-carrying ultrashort pulses and a reference pulse in the temporal frequency domain, provided by the spectral decomposition waves, creates linear phase functions that modulate a readout cw beam by 4WM interaction. The resultant spatial channel output is a sequence of plane waves propagating in directions according to the linear phase functions obtained from the interference of the spectrally decomposed temporal pulses. A Fourier transform focuses the spatial channel output to a sequence of focused spots corresponding to the transmitted signal. The diffracted cw signal is read out with a linear detector array.

In this analysis we use a transform-limited optical short pulse $s(t)$, described by

$$s(t) = p(t - t_0)\exp(j\omega_0 t), \tag{1}$$

where $p(t)$ is the temporal envelope function of the pulse, t_0 is the time location of the pulse peak, and ω_0 is the optical carrier frequency. The pulse's spectrum is found by a Fourier transform of Eq. (1), which yields

$$S(\omega) = P(\omega - \omega_0)\exp[-j(\omega - \omega_0)t_0], \tag{2}$$

where $P(\omega)$ is the Fourier transform of the envelope function $p(t)$. Next we describe and analyze the parallel-to-serial transmitter for an incident pulse spectrum of the form of Eq. (2).

A. Temporal Output of the Parallel-to-Serial Transmitter

To evaluate the system frequency response, consider a monochromatic plane wave of frequency ω incident upon the first reflecting grating at an inclination angle θ (see plane 1 in Fig. 1). The grating is arranged to diffract the carrier frequency component ω_0 into the direction of the optical axis of the system. Thus the diffracted optical field of frequency ω is a plane

wave propagating at a frequency-dependent angle with respect to the optical axis, given by

$$s_1(x;\omega) = \exp\left[-j\,\frac{(\omega-\omega_0)}{c}\,\alpha x\right] w(x), \tag{3}$$

where $\alpha = \sin\theta$, $w(x)$ is the pupil function of the reflecting grating, and c is the speed of light in vacuum. The pupil function $w(x)$ is defined by either the field distribution of the light on the grating or the physical size of the grating surface, whichever is smaller. The field in plane 2 is determined by the spatial Fourier transform of the field in plane 1, yielding

$$s_2(f_x;\omega) = W\left[f_x + \frac{(\omega-\omega_0)}{2\pi c}\,\alpha\right], \tag{4}$$

where $W(f_x)$ is the spatial Fourier transform of $w(x)$, $f_x = [(\omega\tilde{x})/(2\pi cF)]$ is the spatial frequency, F is the lens focal length, and $\tilde{x}$ is the Cartesian coordinate in plane 2. This results in an off-axis spot, in which the spot location depends on the temporal frequency and the spot size depends on the size of the input pupil. Equation (4) shows that, as the temporal frequency of the incident wave deviates from the frequency ω_0, its spatial Fourier transform is shifted in the spatial frequency domain f_x. Furthermore, if a short optical pulse is introduced into the system, it will be spatially dispersed in the Fourier transform plane, where each spectral component will occupy a width determined by the function $W(f_x)$, shifted by the frequency-dependent increment $[(\omega-\omega_0)/(2\pi c)]\alpha$.

Let a 4WM crystal be placed in the Fourier plane of the transmitter to function as a real-time hologram, enabling real-time interchange between the spatial frequency and the temporal frequency domains.[5] The hologram contains information on the interference of the spatial Fourier transform of a reference point source and a sequence of equally spaced mutually coherent point sources in which each point corresponds to a single bit of data (see Fig. 1). The hologram serves as a linear phase filter with transmittance

$$t(f_w) = \sum_n A_n \exp(j2\pi n\Delta f_w), \tag{5}$$

where A_n is the binary amplitude of the nth bit in the spatial data array (either 1 or 0), Δ is the spatial separation between adjacent point sources in the data array, and $f_w = [(\omega_w\tilde{x})/(2\pi cF)]$ is the spatial frequency for a cw writing beam of optical frequency ω_w used in the 4WM arrangement. To use the hologram transmittance function to modulate the short pulse spectrum by the corresponding data, the spatial frequency f_w coordinate of Eq. (5) has to be converted to the frequency f_x of the temporal channel [see Eq. (4)]. By equating the Cartesian coordinate $\tilde{x}$ on the same Fourier plane (see Fig. 1), we obtain the relation $f_x/\omega = f_w/\omega_w$, yielding Eq. (5) in the form

$$t(f_x) = \sum_n A_n \exp\left(j2\pi n\Delta\,\frac{\omega_w}{\omega}\,f_x\right). \tag{6}$$

The ratio ω_w/ω will account for the difference in diffraction of the broad spectrum of a short pulse on a constant spatial frequency grating recorded by a cw frequency source.

The field behind the hologram in plane 2 is $s_2'(f_x;\omega) = s_2(f_x;\omega)t(f_x)$, with $s_2(f_x;\omega)$ and $t(f_x)$ from Eqs. (4) and (6), respectively. A spatial Fourier transform of the field $s_2'(f_x;\omega)$ yields the optical field in plane 3:

$$s_3(x';\omega) = \sum_n A_n w\left[-x' + n\left(\frac{\omega_w}{\omega}\,\Delta\right)\right] \times \exp\left\{j\,\frac{(\omega-\omega_0)}{c}\,\alpha\left[x' - n\left(\frac{\omega_w}{\omega}\,\Delta\right)\right]\right\}, \tag{7}$$

where the minus sign in $w(-x')$ indicates image inversion. The field in plane 3 is diffracted by the second reflecting grating, yielding the output field propagating in the z'' direction:

$$s_3'(x'';\omega) = \sum_n A_n w''\left[-x'' + n\left(\frac{\omega_w}{\omega}\,\Delta\right)\alpha\right] \times \exp\left[-j\,\frac{n(\omega-\omega_0)\omega_w\Delta}{c\omega}\,\alpha\right], \tag{8}$$

where a coordinate rotation of θ degrees from (x', z') to (x'', z'') is performed. The new pupil function $w''(x'')$ is a projection of the pupil function $w(x')$ onto the x'' coordinate. Equation (8) represents the transfer function of the system for any input frequency. The output field propagates in the z'' direction independently of the frequency variable ω.

To complete the analysis, consider introducing into the input of the system a short optical pulse whose corresponding spectrum is described by Eq. (2). The system output is determined by the inverse temporal Fourier transform (denoted by F_ω^{-1}) of the product of Eqs. (2) and (8):

$$s_0(x'';t) = F_\omega^{-1}\left(\{P(\omega-\omega_0)\exp[-j(\omega-\omega_0)t_0]\} \times \left\{\sum_n A_n w''\left[-x'' + n\left(\frac{\omega_w}{\omega}\,\Delta\right)\alpha\right] \times \exp\left[-j\,\frac{n(\omega-\omega_0)\omega_w\Delta}{c\omega}\,\alpha\right]\right\}\right). \tag{9}$$

Equation (9) represents the complete spatial–temporal output of the transmitter.

Next we attempt to simplify the nonlinearity of the frequency response caused by the $1/\omega$ term when the function $P(\omega-\omega_0)$ is bandlimited with a bandwidth of $\Delta\omega$. Let frequency ω be replaced with $\omega_0 + \delta\omega$,

with $\delta\omega \ll \omega_0$, such that the following approximation holds:

$$\frac{1}{\omega} = \frac{1}{\omega_0 + \delta\omega} = \frac{1}{\omega_0}\left[1 - \frac{\delta\omega}{\omega_0} + O\left(\frac{\delta\omega^2}{\omega_0^2}\right)\right] \cong \frac{1}{\omega_0} - \frac{\delta\omega}{\omega_0^2}. \tag{10}$$

The assumption that $1/\omega$ can be accurately approximated by the right-hand side of Eq. (10) will be valid for bandwidths $\Delta\omega$ as large as 10% of the optical carrier (corresponding to a 1% error in the limit). This linearization approach is the novelty of this analysis, since the previous solutions simplified the nonlinearity by replacing ω with ω_0.[7] The previous analysis results are valid for relatively long ultrashort pulses (hundreds of femtoseconds and longer time duration). For shorter pulses, we derive our new result obtained from Eq. (9) with the approximation of Eq. (10), which yields

$$s_0(x''; t) = F_\omega^{-1}\Bigg([P(\delta\omega)\exp(-j\delta\omega t_0)] \times \left\{\sum_n A_n w''\left(-x'' + n\Delta'' - n\Delta''\frac{\delta\omega}{\omega_0}\right) \times \exp\left[-j\frac{n\delta\omega\Delta''}{c} + j\frac{n(\delta\omega)^2\Delta''}{c\omega_0}\right]\right\}\Bigg), \tag{11}$$

where we define $\Delta'' \equiv [(\alpha\omega_w\Delta)/\omega_0]$. The results of Eq. (11) show that our new approximation introduced two additional terms that are not present in the previous analysis. The third term in the aperture function $w''(\cdots)$ will give rise to a frequency-dependent aperture shift, and the second term in the imaginary exponent imposes a chirp function across the bandwidth of the pulse.

To obtain an analytic form for the temporal output, we assume, as an example, a transform-limited Gaussian pulse shape with time constant τ and its corresponding Fourier transform pair given by

$$p(t) = \exp\left(-\frac{t^2}{2\tau^2}\right) \overset{FT}{\Leftrightarrow} P(\omega) = \sqrt{2\pi}\tau\exp\left(-\frac{\tau^2\omega^2}{2}\right). \tag{12}$$

The output of the transmitter with the Gaussian shape input pulse yields

$$s_0(x''; t) = \sum_n A_n\sqrt{2\pi}\exp(j\omega_0 t)\int_{-\infty}^{\infty}\tau\exp\left(-\frac{\tau^2\delta\omega^2}{2}\right) \times \exp\left[j\frac{n\Delta''(\delta\omega)^2}{c\omega_0}\right]w''\left(-x'' + n\Delta'' - n\Delta''\frac{\delta\omega}{\omega_0}\right)\exp(j\delta\omega t_n)\mathrm{d}\delta\omega, \tag{13}$$

where $t_n \equiv t - t_0 - n\,(\Delta''/c)$ is the time delay of the nth pulse or bit encoded. The first term in the integrand of Eq. (13) is a Gaussian pulse spectrum (therefore bandlimited), the second term is a quadratic phase term, and the third term accounts for the input aperture, which has some frequency-dependent shifts. We next argue that the input aperture dependence on the frequency can be neglected, since the edge effect will be insignificant compared with the size of the aperture, which is much smaller than the spectrum of the pulse that sets the limits of integration. Therefore the frequency dependence of the aperture is neglected and the aperture function is taken out of the integrand, as it is no longer frequency dependent. A similar justification does not apply to the quadratic phase term. The quadratic phase results in a frequency chirp imposed on the entire pulse spectrum. After the frequency dependence of the aperture is neglected, Eq. (13) can be directly integrated and the output is

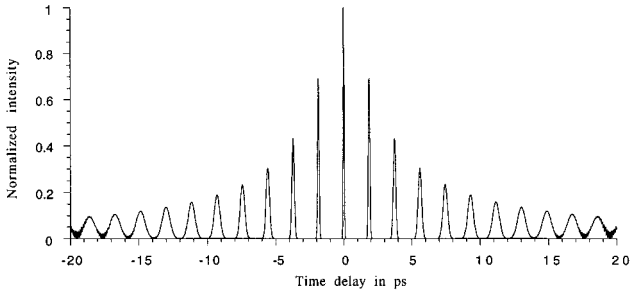

Fig. 3. Time-domain output simulation of parallel-to-serial transmitter. The simulation is shown for a pulse duration of 90 fs, 1.55-μm wavelength, and $\Delta = 0.3$ mm.

$$s_0(x''; t) = \sum_n A_n\exp(j\omega_0 t)w''(-x'' + n\Delta'')\frac{1}{\sqrt[4]{1 + \xi^2 n^2}} \times \exp\left[-j\frac{\tan^{-1}(\xi n)}{2}\right]\exp\left(-\frac{t_n^2}{2\tau^2}\frac{1 + j\xi n}{1 + \xi^2 n^2}\right), \tag{14}$$

where we define the dimensionless parameter $\xi \equiv [(2\Delta'')/(c\omega_0\tau^2)]$. Equation (14) describes a sequence of temporal pulses, each with an aperture position shifted by Δ'', and a temporal separation of Δ''/c, as can be seen in the output of Fig. 1, after plane 3. The peak power of the pulses drops and the duration becomes broader as n increases, preserving the energy in each bit pulse. The phase of the pulses is also varying from pulse to pulse. Since all pulses propagate in the same direction, they can efficiently be coupled into a fiber with a coupling lens. After insertion into a single-mode fiber, the pulse sequence will lose its spatial information, retaining only the temporal properties (pulse separation and broadening). We assume that all n-shifted pupil output pulses are completely coupled into the fiber. The number of pulses that can be completely coupled is the limiting parameter used in calculations of bit-rate capacity in Section 4.

A simulated temporal output for the intensity of a sequence of such pulses in a single mode fiber (with $A_i = 1$ for $\forall i$) is shown in Fig. 3. The information-carrying pulses broaden at the expense of lowering

their peak amplitude as their distance from the center pulse increases.

B. Perfect Reconstruction of a Serial-to-Parallel Receiver

The analysis of the detection process at the receiver shown in Fig. 2 is carried out for the interference of a single pulse from the sequence of pulses defined by Eq. (11) and a reference pulse. The recorded interference pattern is assumed to correspond to only the interference of the data pulse with the reference pulse without intersignal interference (interference between different data pulses in the packet). This assumption is valid as long as the reference pulse power is much stronger than each individual data pulse in the packet. As a consequence of this assumption, we can use the superposition principle and analyze the interference for a single data pulse and then introduce the entire sequence defined by the summation.

The nth received data pulse from Eq. (11) is defined by

$$s_n(t) = F_\omega^{-1}\left\{P(\delta\omega)\exp(-j\delta\omega t_0)A_n \times \exp\left[-j\frac{n\delta\omega\Delta''}{c} + j\frac{n(\delta\omega)^2\Delta''}{c\omega_0}\right]\right\}, \quad (15)$$

where we have dropped the spatial information in the pulse, as it will be lost after pulse transmission through a single-mode fiber. Note that, at this point, we assume that the fiber does not introduce any distortions, a limitation that will be mitigated in Section 3. We therefore model the fiber channel as a perfect channel with a flat frequency response over the bandwidth of the pulse. During the detection, the above data pulse of Eq. (15) interferes at the receiver with the reference pulse:

$$r(t) = p(t)\exp[j\omega_0 t], \quad (16)$$

which has the same pulse envelope as the original short pulse used in the transmitter. The time separation between the reference pulse and the data pulse is now $t_0 + n(\Delta''/c)$ [because of the combination of the two linear phases in Eq. (15)], where t_0 is the time separation between the center of the reference pulse and the center of the data packet, and the second term, $n(\Delta''/c)$, is the time shift of the nth data pulse relative to the center of the data packet (see Fig. 2). The corresponding spectra of the data pulse and the reference pulse are the Fourier transforms of Eqs. (15) and (16),

$$S_n(\omega) = P(\delta\omega)\exp(-j\delta\omega t_0)A_n \times \exp\left[-j\frac{n\delta\omega\Delta''}{c} + j\frac{n(\delta\omega)^2\Delta''}{c\omega_0}\right], \quad (17)$$

$$R(\omega) = P(\delta\omega), \quad (18)$$

respectively, where we use $\omega = \omega_0 + \delta\omega$. Both pulses are introduced into the receiver, where they are both spectrally decomposed by the input grating combined with a spatial Fourier transform lens, again producing the spatially dispersed spectrum on the Fourier plane (plane 2). Following an identical derivation for the system response as was done for the transmitter, the system response is similar to Eq. (4):

$$W(f_x; \omega) = W\left(f_x + \frac{\delta\omega}{2\pi c}\alpha\right), \quad (19)$$

where again,

$$f_x = \frac{(\omega_0 + \delta\omega)x'}{2\pi cF}.$$

The system frequency response [Eq. (19)] multiplies the signal and reference pulses' spectra [Eqs. (17) and (18), respectively] to provide the spatially dispersed spectra on the Fourier plane (plane 2 in Fig. 2).

The output signal resulting from 4WM at the receiver is determined by the intensity variations from the interference of the temporal signals' spectra, which in turn diffract a cw beam. The intensity, given by $|R(\omega)W(f_x; \omega) + S_n(\omega)W(f_x; \omega)|^2$, will have four components that can be separated spatially when a displacement is introduced between the signal and reference in the y direction to provide the desired holographic signal:

$$R(\omega)S_n^*(\omega)|W(f_x; \omega)|^2 = A_n|P(\delta\omega)|^2\exp\left[j\left(t_0 + \frac{n\Delta''}{c}\right)\delta\omega - j\frac{n\Delta''}{c\omega_0}(\delta\omega)^2\right]|W(f_x; \omega)|^2. \quad (20)$$

If we assume that there is no spectral dependency in the hologram within the pulse bandwidth, the recorded holographic signal at every location along x' is given by

$$H_n(x') = \int_{-\infty}^{\infty} R(\omega)S_n^*(\omega)|W(f_x; \omega)|^2 d\omega \quad (21)$$

by substitution of the expression for f_x, as it is a function of ω and x'. A precise derivation of the recorded holographic signal is provided in Appendix A, and a simplified approach is given below. To simplify evaluation of the integral in Eq. (21), we approximate the Fourier-transformed aperture by a Dirac delta function, $W(f_x; \omega) \approx \delta(f_x; \omega)$, which yields

$$H_n(x') = A_n|P(\delta\omega)|^2\exp\left[j\left(t_0 + \frac{n\Delta''}{c}\right)\delta\omega - j\frac{n\Delta''}{c\omega_0}(\delta\omega)^2\right], \quad (22)$$

along with the substitution

$$\delta\omega = -\frac{x'\omega_0}{x' + \alpha F}, \quad (23)$$

which is the relation between the Cartesian coordinate x' and the pulse spectrum derived from the integration over the Dirac delta function. Equation

(23) can be further simplified by a second approximation, similar to that made in the transmitter analysis,

$$\delta\omega = -\frac{x'\omega_0}{\alpha F}\left(\frac{1}{1+\frac{x'}{\alpha F}}\right) = -\frac{x'\omega_0}{\alpha F}\left\{1-\frac{x'}{\alpha F}+O\left[\left(\frac{x'}{\alpha F}\right)^2\right]\right\}$$

$$= -\frac{x'\omega_0}{\alpha F}+\omega_0\left(\frac{x'}{\alpha F}\right)^2+O\left[\left(\frac{x'}{\alpha F}\right)^3\right], \quad (24)$$

$$(\delta\omega)^2 = \left(\frac{\omega_0 x'}{\alpha F}\right)^2+O\left[\left(\frac{x'}{\alpha F}\right)^3\right], \quad (25)$$

as $[x'/(\alpha F)] \ll 1$. When the above expressions are substituted for $\delta\omega$, the spatial variations take the final form of

$$H_n(x') = A_n\left|P\left[-\frac{x'\omega_0}{\alpha F}+\omega_0\left(\frac{x'}{\alpha F}\right)^2\right]\right|^2\exp\left(-j\frac{n\Delta''}{c}\frac{x'\omega_0}{\alpha F}\right)$$
$$\times\exp\left\{j\omega_0 t_0\left[-\frac{x'}{\alpha F}+\left(\frac{x'}{\alpha F}\right)^2\right]\right\}. \quad (26a)$$

The first term in Eq. (26a) describes the power spectrum envelope of the pulse bandwidth, the second term is the linear phase signal that carries the nth-bit information, and the third term accounts for the additional linear phase of the separation t_0 and a distortion term in the form of a quadratic phase. The power spectrum envelope of the recorded hologram serves as an apodization for the readout beam. Its effect is to increase the spot size on the diffracted signal, which will limit the number of bits that can be transmitted by this scheme. This issue is discussed further in Section 4. The linear phase is a function of n, which corresponds to a unique phase function for each data pulse in the packet transmitted. The distortion term depends on the time separation of the reference pulse and the center of the data packet t_0; thus, to eliminate this distortion term, the timing of the reference pulse must be set such that $t_0 = 0$. Finally, a cw plane wave interacting with the real-time spectral hologram will generate a diffraction pattern that coincides with the original transmitted data.

The approximation made in the derivation of Eq. (26a), i.e., $W(f_x; \omega) \approx \delta(f_x; \omega)$, resulted in some loss of information regarding the temporal overlap of pulses in the input pupil function. We reintroduce this lost information by adding the temporal factor $K_n(t)$ to the equation, which yields

$$H_n(x'; t) = A_n\left|P\left[-\frac{x'\omega_0}{\alpha F}+\omega_0\left(\frac{x'}{\alpha F}\right)^2\right]\right|^2$$
$$\times\exp\left(-j\frac{n\Delta''}{c}\frac{x'\omega_0}{\alpha F}\right)$$
$$\times\exp\left\{j\omega_0 t_0\left[-\frac{x'}{\alpha F}+\left(\frac{x'}{\alpha F}\right)^2\right]\right\}K_n(t). \quad (26b)$$

The temporal factor is found in the precise analysis of Appendix A and is given in Eq. (A7) as

$$K_n(t) \cong w\left(\frac{ct}{\alpha}\right)w\left[\frac{c}{\alpha}\left(t-t_0-\frac{n\Delta''}{c}\right)\right].$$

The temporal factor determines how long the interference pattern would exist between a reference pulse and a pulse separated in time by $t_0 + [(n\Delta'')/c]$.

Similar to the example in Subsection 2.A, consider again a transform-limited Gaussian pulse shape with time constant τ. When the spectrum of the Gaussian pulse is substituted into Eq. (26b), the spatiotemporal signal is

$$H_n(x'; t) = A_n\exp\left[-\tau^2{\omega_0}^2\left(\frac{x'}{\alpha F}\right)^2\right]\exp\left(-j\frac{n\Delta''}{c}\frac{x'\omega_0}{\alpha F}\right)$$
$$\times\exp\left\{jt_0\left[-\frac{x'\omega_0}{\alpha F}+\omega_0\left(\frac{x'}{\alpha F}\right)^2\right]\right\}K_n(t). \quad (27)$$

The spatial intensity variations in the crystal are read out by a cw beam in a 4WM configuration, with a temporal envelope determined by $K_n(t)$. The readout cw beam of wavelength λ_r diffracts from the intensity-induced spatial variations, and after a Fourier transform results in the output field on plane 3 in Fig. 2 (assuming no distortion by setting $t_0 = 0$):

$$h(x^\dagger; t) = \sum_n h_n(x^\dagger; t)$$
$$= \sum_n A_n\exp\left[-\frac{\alpha^2\left(\frac{x^\dagger}{\lambda_r}+\frac{n\Delta''}{\alpha\lambda_0}\right)^2}{4\tau^2{\omega_0}^2}\right]K_n(t), \quad (28)$$

which is a collection of Gaussian spots separated in space. The location of the signal of each data point is at $x^\dagger = -n\Delta(\lambda_r/\lambda_w)$, where λ_w is the cw wavelength used to write the phase function in the transmitter. The energy at each diffracted signal (defined by intensity times time) is determined by integration of the temporal factor, which is equivalent to the autocorrelation function of the pupil function evaluated at a lag of $(n\Delta'')/c$. As $|n|$ increases, less energy is available for detection at the output.

3. Dispersion Compensation Property of Serial-to-Parallel Receiver

The preceding analysis treated the transmission medium as a perfect channel. The transmitted signals did not experience any distortion between the transmitter and the receiver, where the data are interfered with by a reference pulse for detection. If the data were corrupted by the transmission, and a local reference pulse would be interfered with for detection at the receiver, the detected data would be distorted. However, when the reference pulse is sent over the same optical fiber along with the data, both signals experience the same distortion effect, and, by the phase-conjugation process inherently present in the 4WM technique, the readout beam compensates for the distortion.

Let the signal $s(t)$ and the reference pulse $r(t)$ propagate in a fiber. The fiber introduces distortions to the pulses because of dispersion, absorption, scattering, mechanical stress, and temperature fluctuations, all of which can be modeled as $a(\omega)\exp[j\Phi(\omega)]$, where $a(\omega)$ and $\exp[j\Phi(\omega)]$ account for the transmittance and the acquired phase, respectively. This distortion model excludes nonlinear, intensity-dependent phenomena and implicitly assumes a time-invariant response on the time scale of packet time duration. The acquired phase is canceled by the conjugation of the signal and reference pulses in the 4WM process with the holographic signal of interest:

$$\{R(\omega)a(\omega)\exp[j\Phi(\omega)]W(x';\omega)\} \times \{S(\omega)a(\omega)\exp[j\Phi(\omega)]W(x';\omega)\}^* = R(\omega)S^*(\omega)|a(\omega)|^2|W(x';\omega)|^2. \quad (29)$$

This result is nearly identical to that of the ideal channel, illustrating the dispersion compensation property of this transmission scheme. The acquired phase term has been compensated for by the phase conjugation. The effect of the frequency selectivity in the fiber transmittance serves to enhance further the apodization of the energy profile, similar to the effect of the power spectrum discussed in Subsection 2.B. This would affect the diffracted orders' spot size.

An additional benefit of transmitting the reference pulse along with the data is the self-referencing in the receiver. Since the reference pulse does not have to be generated in the receiver, no timing errors can occur, and with proper alignment, the $t_0 = 0$ condition can be easily satisfied, guaranteeing proper synchronization of the system.

Since the reference pulse can be made much stronger than the data pulses, it can be also used in direct detection for signaling the receiver circuitry to acquire the data from the detector array, thus synchronizing the receiver detection circuitry to the transmitted data. The number of data bits that can be transmitted in a single packet is discussed in Section 4.

4. Bit-Rate Capacity of Transmission System

Several system assumptions have to be made in order to calculate the aggregate bit-rate capacity of this transmission link. The capacity, in bits per second, is the number of bits that can be encoded onto a single ultrashort pulse multiplied by the repetition rate of the system. In our model we assume a center wavelength of 1.55 μm for low attenuation and new all-fiber ultrashort laser sources at this wavelength.[12] The transmission medium is a single-mode fiber so that modal dispersion can be neglected.

Two criteria have to be satisfied to couple the output data pulses efficiently into a single-mode fiber (see Fig. 4): (1) The output beams' focused spot sizes have to be comparable with the mode field diameter of the optical fiber, and (2) the focused beams have to arrive from directions that lie within the N.A. of the fiber. The coupling-lens focal length F' is chosen

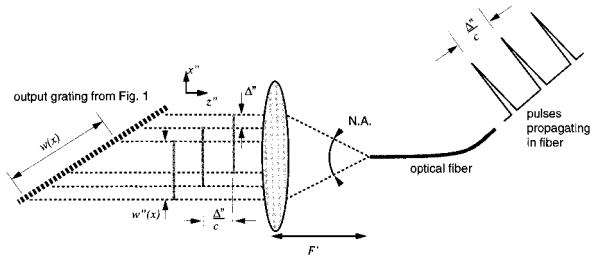

Fig. 4. Coupling output pulses of transmitter into an optical fiber. The output pulses, of the size of $w''(x)$, are delayed by Δ''/c and laterally shifted by Δ''. Lens F' couples the pulses into a fiber, where the lateral shift information is lost.

according to the spot-size criteria, such that each output beam width, determined by the projection of the input pupil $w''(x)$, is focused to the mode field diameter of the fiber. For a chosen focusing lens F', the number of channels that can be collected M is found in paraxial approximation by simple trigonometry:

$$M = \frac{F'\text{N.A.}}{\Delta''}, \quad (30)$$

where we assume that the fiber coupling behaves as a hard-clipped function (i.e., the light will be completely coupled if it is within the N.A.).

For determining the minimum spatial shift of the pulses Δ'' that will maximize the capacity, the receiver output spatial channels need to be separated enough to create low cross talk in the detector array. As discussed in Section 3, a plane wave illuminating the recorded interference pattern in the receiver will diffract to different locations. The spot size of the diffracted signals and their separation will determine Δ''. The allowable cross-talk power is chosen to be -20 dB and is generated mainly from adjacent channels. We assume that the temporal factor attenuation plays a negligible role in cross-talk evaluation, as the attenuation difference between adjacent pulses is small when the pupil function is designed to include many pulses (i.e., temporal length of pupil function is

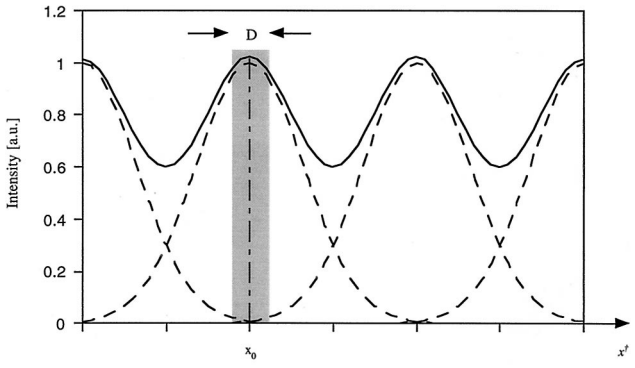

Fig. 5. Intensity output of diffracted data points. Spots are displaced by x_0, a distance that guarantees a signal-to-cross-talk ratio of 20 dB. The shaded area corresponds to light intensity gathered by a detector of width D.

large compared with pulse separation, Δ''/c). For our example of a Gaussian pulse input, with negligible transmission losses and with $t_0 = 0$, the diffracted output signal is given by Eq. (28), which is a collection of Gaussian spots separated in space (see Fig. 5). The spatial location of the signal of the nth data pulse is given by $x^{\dagger} = -n\Delta(\lambda_r/\lambda_w)$. The signal-to-cross-talk ratio (SXR) is defined by the ratio of the signal power integrated on a detector of width D to that of the cross-talk power on the same detector from the adjacent channels. For Gaussian signals the SXR is given by

$$\mathrm{SXR} = \frac{\operatorname{erf}\left(\frac{\alpha}{2\tau\omega_0\lambda_r}\frac{D}{\sqrt{2}}\right)}{\operatorname{erf}\left[\frac{\alpha}{\sqrt{2}\tau\omega_0}\left(\frac{\Delta}{\lambda_w}+\frac{D}{2\lambda_r}\right)\right]-\operatorname{erf}\left[\frac{\alpha}{\sqrt{2}\tau\omega_0}\left(\frac{\Delta}{\lambda_w}-\frac{D}{2\lambda_r}\right)\right]+2\exp\left[-\frac{1}{2}\left(\frac{\alpha\Delta}{\lambda_w\omega_0\tau}\right)^2\right]\operatorname{erf}\left(\frac{\alpha}{2\tau\omega_0\lambda_r}\frac{D}{\sqrt{2}}\right)}, \tag{31}$$

which is a monotonically decreasing function of the detector width D. When Δ is numerically solved to obtain the specified SXR of 20 dB, with a transmission wavelength $\lambda_0 = 1.55$ μm, readout wavelength $\lambda_r = 1.55$ μm, writing wavelength $\lambda_w = 0.5$ μm, $\alpha = 0.6$, pulse duration 90 fs (for a time constant of $\tau = 54$ fs), and detector width $D = 50$ μm, the value found is $\Delta = 190$ μm. The separation of the spatial channels in the transmitter, Δ, is within the practical range of spatial light modulator technology. Inserting this value into Eq. (30), after converting to Δ'', we find that the number of pulses that can be encoded and reliably detected in a packet is $M = 31$. For this calculation we assume a standard single-mode fiber with a mode field diameter of 9.3 μm, a N.A. of 0.11, and a 100-mm focal-length lens that can efficiently couple the beams. For a laser repetition rate of 100 MHz, the aggregate data rate is the pulse repetition rate times M, which is 3.1 Gbits/s for the example assumed.

Noting that a transform-limited Gaussian pulse of 90-fs duration has a bandwidth of 4.9 THz, we are clearly not utilizing the bandwidth efficiently. Yet this scheme still leaves ample room for time-division multiplexing, as the packet duration $\{[(M\Delta'')/c] = 36.5$ ps$\}$ is much shorter than the packet repetition time (1/100 MHz = 10 ns). When other users are introduced into a time-division-multiplexing network environment, each with access to a 36-ps window within a 10-ns frame, with guard bands between packets of half a packet's duration, approximately 185 users can share the fiber link, for a total aggregate rate of 573.5 Gbits/s.

The data rate derived above is by no means a bound on the possible rate. A larger focusing lens F', along with a larger pupil function on the gratings, wavelength variations, and other parameters, can increase the rate further. A detailed design must not conflict with the assumption made, i.e., that the energy in the bits is enough for 4WM yet not high enough to stimulate nonlinear phenomena in the fiber.

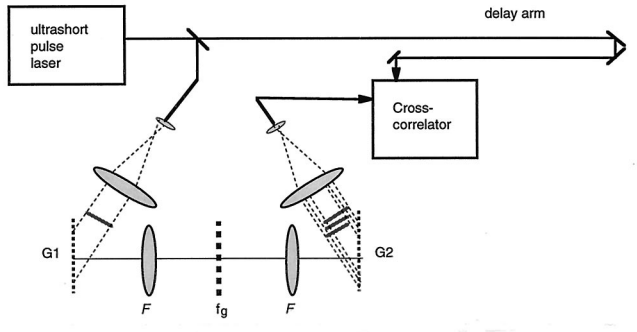

Fig. 6. Schematic of experiment setup. G's, dispersion gratings; f_g, Ronchi grating.

5. Experimental Results of Temporal Output Measurements

Previous experiments have verified time-to-space conversions,[5] space-to-time conversions,[6] and a complete space–time–space transmission.[7] The analysis in Subsection 2.A presents a new result in the temporal output of space-to-time conversions [Eq. (14)], which predicts chirping of the output pulses, in which the amount of chirp depends on the slope of the linear phase function and the pulse bandwidth.

The anticipated chirping of the output pulses from the parallel-to-serial transmitter were verified experimentally by cross-correlation measurements (see Fig. 6). In this experiment, a short pulse from a Coherent Mira 900 laser [$\lambda_0 = 0.92$ μm and $\tau = 93$ fs, assuming a Gaussian pulse as described by Eq. (12)] is split by a beam splitter into two arms. One arm includes a pulse shaper that simulates the transmitter, and the second is an equal-length delay arm.

Table 1. Calculated and Experimental Results of the FWHM for 20-, 28-, and 39-lp/mm Gratings

Frequency (lp/mm)	Calculated FWHM	Measured FWHM	Standard Deviation of Measurement	Error
−39	0.4929	0.4861	0.0071	0.0068
−28	0.3856	0.3823	0.0084	0.0033
−20	0.3156	0.2837	0.0023	0.0319
0	N/A	0.2192	0.0044	N/A
20	0.3156	0.3003	0.0024	0.0153
28	0.3856	0.3924	0.0064	−0.0068
39	0.4929	0.4859	0.0111	0.0070

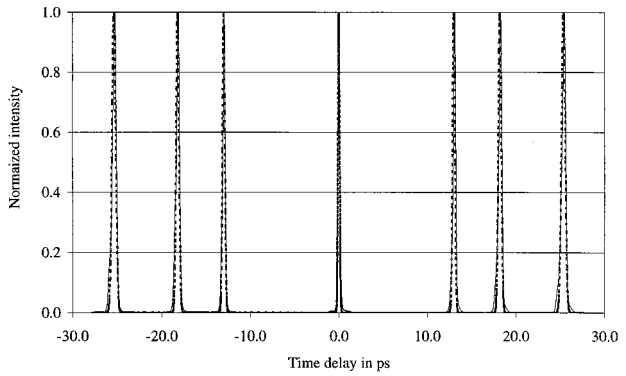

Fig. 7. Plot of the cross-correlation traces. The solid curves are the measured curves, and the dashed curves are the theoretical curves.

The pulse shaper has 600-lp/mm gratings (lp/mm is line pairs per millimeter) in an optical $4F$ setup. The linear phase functions in the spectral plane were generated by amplitude Ronchi gratings, whose Fourier series decomposition reveals that the 0 and the ± 1 orders are predominant. Therefore the output signal for each grating consisted of three strong pulses, the original transform-limited pulse and the two signal pulses, one preceding and one trailing the transform-limited pulse. In this experiment we did not consider higher-order diffracted beams. One of these pulses is up chirped, and the second is down chirped. This output was analyzed by an intensity cross correlation (Inrad Auto-correlator 514-BX modified for cross-correlation measurements) with the original transform-limited pulse in the delay arm.

The FWHM value was used as a basis for comparison between the calculated and the measured results. The nondiffracted signal was used to measure the FWHM of the transform-limited pulse and to obtain the value of τ. Each measurement was taken five times and averaged. Three different Ronchi gratings of varying frequencies, i.e., 20, 28, and 39 lp/mm, were used as the spectral filters in the pulse shaper. Experimental results are summarized in Table 1, and the superimposed traces of all the measurements are shown in Fig. 7. Each cross-correlation trace was individually scaled for a peak intensity of 1, as each correlation was a different measurement that required an adjustment of the gain in the detector.

Some variations in the waveforms of the measured and the theoretical pulses are shown. In general, the measured autocorrelation curve diverges slightly from the Gaussian profile. This divergence can be accounted for by the fact that the Gaussian model does not fit precisely the pulse shape, and other pulse-shape models could provide a better fit (e.g., hyperbolic secant). Furthermore, the cross correlations reveal an asymmetry consistently to one side of the data. This can be attributed to third-order dispersion through glass elements such as the lenses used in the pulse-shaping device.

From the tabulated results, we see that the calculated and the measured values are in excellent agreement. The error and the standard deviation of the measurements are of the same magnitude, except for the lowest-frequency grating, for which the calculated FWHM is 8% higher. This experiment proves that the output pulses are chirped, as expected by the theoretical analysis of Subsection 2.A.

6. Summary

An analysis of a transmission method based on parallel-to-serial transmitters and serial-to-parallel receivers has been presented. The transmitted signal is in a format of data packets, consisting of a sequence of pulses, each representing a bit with ON–OFF keying. We show that the pulses in the packet have different amounts of chirp, depending on the pulse location in the packet. However, this chirping phenomenon, predicted and experimentally measured by this analysis, does not affect the reconstruction ability of our receiver, because the serial data are converted back to parallel channels by our coherent detection scheme based on 4WM at the receiver. Furthermore, when the reference pulse is transmitted along with the data on the same optical fiber, the effects of accumulated phase distortions are self-compensated for by the phase-conjugation process inherent in the 4WM technique. Additionally, this method provides self-referencing, as no reference pulse has to be generated in the receiver. This may solve timing errors that occur when a local reference pulse has to be supplied at the receiver, which has been shown to cause distortion of the reconstructed signal.

This scheme, however, relies on real-time holographic material, which presents a challenge as well. A complete transmission system has been experimentally constructed by use of ferroelectric photorefractives, as a proof of concept.[7] This group of materials requires a recording time of the order of seconds, clearly eliminating them from practical systems. Current research on semiconductor multiple-quantum-well photorefractives is producing material with a much faster response time.[13,14] Yet realistic implementations will undoubtedly need to rely on electronic $\chi^{(3)}$ nonlinearities for almost instantaneous response times in a 4WM configuration. To access such nonlinearities, high-power beams are required, which conflict with the requirement that the transmitted beams be of low enough power not to stimulate nonlinearities in the optical fiber. One possible solution to this problem is to amplify the optical signal near the receiver such that the transmission would not incur distortions yet the received signal would be strong enough to excite $\chi^{(3)}$ nonlinearities. Another solution may be to chirp the pulses intentionally to lower their peak powers for transmission in a fiber and to recompress or dechirp at the receiver, increasing the instantaneous power before the nonlinear 4WM process.

Appendix A

In this appendix we rederive the perfect reconstruction receiver (Section 2.B) in the temporal domain, as opposed to the temporal frequency domain approach utilized above. Using this approach, we find the time factor $K_n(t)$ that dictates how long the interference pattern on the real-time holographic material will exist.

We begin with the field distribution in the mixed spatiotemporal domain of the reference pulse. The field is given as the product of Eqs. (18) and Eq. (19):

$$U_r(f_x;\omega) = P(\omega-\omega_0)W\left(f_x + \frac{\omega-\omega_0}{2\pi c}\alpha\right), \quad \text{(A1)}$$

where $f_x = [(\omega\tilde{x})/(2\pi cF)]$ is frequency dependent. To find the temporal variations, we perform an inverse temporal Fourier transform:

$$U_r(x';t) = \frac{1}{2\pi}\int_{-\infty}^{\infty} P(\omega-\omega_0)W\left(\frac{\omega x'}{2\pi cF} + \frac{\omega-\omega_0}{2\pi c}\alpha\right) \times \exp(j\omega t)\mathrm{d}\omega, \quad \text{(A2)}$$

where we have switched to the real coordinate x'. To simplify the Fourier integral of Eq. (A2), we note that the pupil function $W(\cdots)$ is bandlimited relative to the pulse spectrum, and we can therefore pull the spectral function $P(\cdots)$ out of the integral and substitute for the value $\omega - \omega_0$ the location dependence according to the pupil function. This simplification results in

$$U_r(x';t) = \frac{1}{2\pi}P\left(-\frac{\omega_0 x'}{x'+\alpha F}\right)\int_{-\infty}^{\infty} W\left[\frac{\omega x'}{2\pi cF} + \frac{\omega-\omega_0}{2\pi c}\alpha\right)\exp(j\omega t)\mathrm{d}\omega. \quad \text{(A3)}$$

Solving this integral is trivial at this point, and after its solution we simplify the relation of the Cartesian coordinate x' in the pulse spectrum by Eq. (24), yielding

$$U_r(x';t) = P\left[-\frac{\omega_0 x'}{\alpha F} + \omega_0\left(\frac{x'}{\alpha F}\right)^2\right]\frac{c/\alpha}{1+\frac{x'}{\alpha F}} \times \exp\left\{j\omega_0 t\left[1-\frac{x'}{\alpha F}+\left(\frac{x'}{\alpha F}\right)^2\right]\right\} w\left(\frac{ct/\alpha}{1+\frac{x'}{\alpha F}}\right). \quad \text{(A4)}$$

Equation (A4) is recognized as the field description of spectrally dispersed waves, which have a finite time of existence, defined by the pupil function, and the propagation direction is time varying.

The field distribution for the signal pulse can be found in a similar manner, resulting in

$$U_s(x';t) = A_n P\left[-\frac{\omega_0 x'}{\alpha F} + \omega_0\left(\frac{x'}{\alpha F}\right)^2\right]\frac{c/\alpha}{1+\frac{x'}{\alpha F}} \times \exp\left\{j\omega_0 t\left[1-\frac{x'}{\alpha F}+\left(\frac{x'}{\alpha F}\right)^2\right]\right\} \times \exp\left\{j\omega_0 t_0\left[\frac{x'}{\alpha F}-\left(\frac{x'}{\alpha F}\right)^2\right]\right\} \times \exp\left(j\omega_0\frac{n\Delta''}{c}\frac{x'}{\alpha F}\right) w\left[\frac{c\left(t-t_0-\frac{n\Delta''}{c}\right)\Big/\alpha}{1+\frac{x'}{\alpha F}}\right]. \quad \text{(A5)}$$

The intensity distribution on the real-time holographic material is given by $|U_s(x';t) + U_r(x';t)|^2$, and the holographic signal of interest $U_s^*(x';t)U_r(x';t)$ is

$$U_s^*(x';t)U_r(x';t) = A_n\left|P\left[-\frac{\omega_0 x'}{\alpha F} + \omega_0\left(\frac{x'}{\alpha F}\right)^2\right]\right|^2 \times \left(\frac{c/\alpha}{1+\frac{x'}{\alpha F}}\right)^2 \exp\left(-j\omega_0\frac{n\Delta''}{c}\frac{x'}{\alpha F}\right) \times \exp\left\{j\omega_0 t_0\left[-\frac{x'}{\alpha F}+\left(\frac{x'}{\alpha F}\right)^2\right]\right\} \times K_n(x';t), \quad \text{(A6)}$$

where

$$K_n(x';t) = w\left(\frac{ct/\alpha}{1+\frac{x'}{\alpha F}}\right) w\left[\frac{c\left(t-t_0-\frac{n\Delta''}{c}\right)\Big/\alpha}{1+\frac{x'}{\alpha F}}\right] \cong w\left(\frac{ct}{\alpha}\right) w\left[\frac{c\left(t-t_0-\frac{n\Delta''}{c}\right)}{\alpha}\right] \equiv K_n(t). \quad \text{(A7)}$$

The result derived in this Appendix, Eq. (A6), is similar to the result in Eq. (26a), apart from the temporal variation factor $K_n(t)$ and a nearly constant factor term. The temporal factor multiplies the output interference signal by a function that measures the time at which both the signal and the reference pulses overlap on the input pupil function. As the temporal separation of the two pulses increases {i.e., $|t_0 + [(n\Delta'')/c]|$ is larger}, a real-time 4WM output signal will exist for a shorter time, and therefore less energy will reach the detector.

This study was supported in part by the Focused Research Initiative of the Ballistic Missile Defense Organization, the U.S. Air Force Office of Scientific

Research, and the U.S. National Science Foundation. D. Marom acknowledges the support of the Fannie and John Hertz Foundation.

References

1. C. Froehly, B. Colombeau, and M. Vampouille, "Shaping and analysis of picosecond light pulses," in *Progress in Optics*, E. Wolf, ed. (North-Holland, Amsterdam, 1983), Vol. XX, pp. 65–153.
2. A. M. Weiner, J. P. Heritage, and E. M. Kirschner, "High-resolution femtosecond pulse shaping," J. Opt. Soc. Am. B **5,** 1563–1572 (1988).
3. Y. T. Mazurenko, "Holography of wave packets," Appl. Phys. B **50,** 101–113 (1990).
4. A. M. Weiner, D. E. Leaird, D. H. Reitze, and E. G. Paek, "Femtosecond spectral holography," IEEE J. Quantum Electron. **28,** 2251–2261 (1992).
5. M. C. Nuss and R. L. Morrison, "Time-domain images," Opt. Lett. **20,** 740–742 (1995).
6. M. C. Nuss, M. Li, T. H. Chiu, A. M. Weiner, and A. Patrovi, "Time-to-space mapping of femtosecond pulses," Opt. Lett. **19,** 664–666 (1994).
7. P. C. Sun, Y. Mazurenko, W. S. C. Chang, P. K. L. Yu, and Y. Fainman, "All optical parallel-to-serial conversion by holographic spatial-to-temporal frequency encoding," Opt. Lett. **20,** 1728–1730 (1995).
8. K. Ema, M. Kuwata-Gonokami, and F. Shimizu, "All-optical sub-Tbits/s serial-to-parallel conversion using excitonic giant nonlinearity," Appl. Phys. Lett. **59,** 2799–2801 (1990).
9. Yu. T. Mazurenko, A. G. Spiro, S. E. Putilin, and A. G. Belyaev, "Ultrafast space-time transformation of signals using spectral nonlinear optics," Opt. Spectrosc. (USSR) **78,** 122–128 (1995).
10. Yu. T. Mazurenko, A. G. Spiro, S. E. Putilin, A. G. Beliaev, and E. B. Verkhovskij, "Time-to-space conversion of fast signals by the method of spectral nonlinear optics," Opt. Commun. **118,** 594–600 (1995).
11. P. C. Sun, Yu. T. Mazurenko, and Y. Fainman, "Femtosecond pulse imaging: ultrafast optical oscilloscope," J. Opt. Soc. Am. A **14,** 1159–1170 (1997).
12. H. A. Haus, K. Tamura, L. E. Nelson, and E. P. Ippen, "Stretched-pulse additive pulse mode-locking in fiber ring lasers: theory and experiment," IEEE J. Quantum Electron. **31,** 591–598 (1995).
13. R. M. Brubaker, Q. N. Wang, D. D. Nolte, E. S. Harmon, and M. R. Melloch, "Steady-state four-wave mixing in photorefractive quantum wells with femtosecond pulses," J. Opt. Soc. Am. B **11,** 1038–1044 (1994).
14. A. Patrovi, A. M. Glass, D. H. Olsen, G. J. Zydzik, H. M. O'Bryan, T. H. Chiu, and W. H. Knox, "Cr-doped GaAs/AlGaAs semi-insulating multiple quantum well photorefractive devices," Appl. Phys. Lett. **62,** 464–466 (1993).